Magnetic polaron and unconventional magnetotransport properties of the single-crystalline compound EuBiTe₃

Wonhyuk Shon and Jong-Soo Rhyee[*]
Department of Applied Physics and Institute of Applied Sciences, Kyung Hee University, Yongin 17104, Korea

Yingshi Jin and Sung-Jin Kim
Department of Chemistry and Nano Science, Ewha Womans University, Seoul 03760, Korea

We investigate the magnetic, thermal, and electrical transport properties on the single-crystalline compound EuBiTe₃. The magnetization measurements reveal the antiferromagnetic transition at 7 K along the *ab* plane with a stable Eu^{2+} ion. A short-range ferromagnetic interaction along the *c* axis is inferred from magnetic susceptibility and heat capacity measurements, which we associate with the presence of magnetic polarons. The magnetic polaron gives rise to unconventional negative magnetoresistance such as the weak antilocalization (WAL) and weak localization crossover. The WAL of the angle-resolved magnetoconductivity is well described by the Al'tshuler and Aronov model along the longitudinal magnetoconductivity. The magnetic polaron is widely observed above Néel temperature up to 50 K, which is supported by the Majumdar-Littlewood model in a scaled magnetoresistance. Even though EuBiTe₃ should have one hole per formula unit, the electrical conductivity $\sigma(T)$ exhibits strong localized insulating behavior. The transport mechanism of $\sigma(T)$ is distinguished by two different mechanism: Efros-Shklovskii-type variable range hopping (VRH) transport in the high-temperature range ($T \geqslant 52$ K) and three-dimensional VRH transport in the low-temperature regime ($T \leqslant 50$ K). The VRH transport suggests that the insulating behavior of $\sigma(T)$ on the compound can originate from a Mott-type insulator with strong Coulomb interaction.

I. INTRODUCTION

In the past decade, the topological state of matter has been intensively investigated in condensed-matter physics [1–3]. A topological insulator has a topologically protected gapless surface state with an insulating bulk gap [4]. The topological state can exist in various strongly correlated and interacting spin systems such as the topological Kondo insulator [5,6], the antiferromagnetic topological insulator [7,8], the topological Mott insulator [9], the topological Anderson insulator [10], etc. Because the topological state is based on strong spin-orbit coupling, there have been significant efforts to find new topological materials with strong spin-orbit coupling.

Rare-earth ternary chalcogenides are one of the candidate systems for exotic states of matter because of strong spin-orbit coupling and magnetic interaction among localized *f* electrons. RBiTe₃ (R is a rare-earth element) compounds can be regarded as homologous compounds in which the rare-earth element R replaces one of the quintuple Bi layers in Bi₂Te₃. The theoretical *ab initio* calculation predicted that LaBiTe₃ can be a strong topological insulator [11], where the crystal structures of LaBiTe₃, YBiTe₃, LaSbTe₃, and YSbTe₃ share the same rhombohedral crystal structure with the space group $R\bar{3}m$. In addition, the noncentrosymmetric three-dimensional topological insulators LaBiTe₃ and LuBiTe₃ can undergo a topological phase transition from a topological insulator to a normal insulator in the intermediate range of Sb-doped LaBi$_{1-x}$Sb$_x$Te₃ and LuBi$_{1-x}$Sb$_x$Te₃ for $x = 38.5\%$–41.9% and $x = 40.5\%$–45.1%, respectively [12]. Liu *et al.* argued that there should be a Weyl semimetallic state near the topological phase transition in the intermediate doping range [12]. However, it has not yet been proved by experimental investigations.

Recently, single-crystalline compounds EuBiTe₃ and EuSbTe₃ were synthesized using the flux method which have orthorhombic crystal structure and an antiferromagnetic transition at $T_N = 7.6$ K [13]. EuBiTe₃ can be applied to the broadband photodetector, which is operated at room temperature in the wavelength range from ultraviolet (370 nm) to near infrared (1550 nm) with good reproducibility [14]. A possible magnetic polaron on the EuBiTe₃ compound [13] was also proposed. A magnetic polaron is a metastable quasiparticle which is a bound ferromagnetic cluster within an antiferromagnetic or paramagnetic background [15–17]. The weak ferromagnetic ordering of a magnetic polaron along a specific direction gives abnormal magnetotransport properties [18–20].

Here we investigate the magnetic, thermal, and magnetotransport properties of the compound EuBiTe₃ and interpret the unconventional magnetotransport by the formation of a magnetic polaron. We observe a small kink in magnetization $M(H)$ curves at low temperatures, implying a hidden magnetic interaction under the antiferromagnetic background. The magnetotransport properties of the compound EuBiTe₃ also support the ferromagnetic polaron formation. The
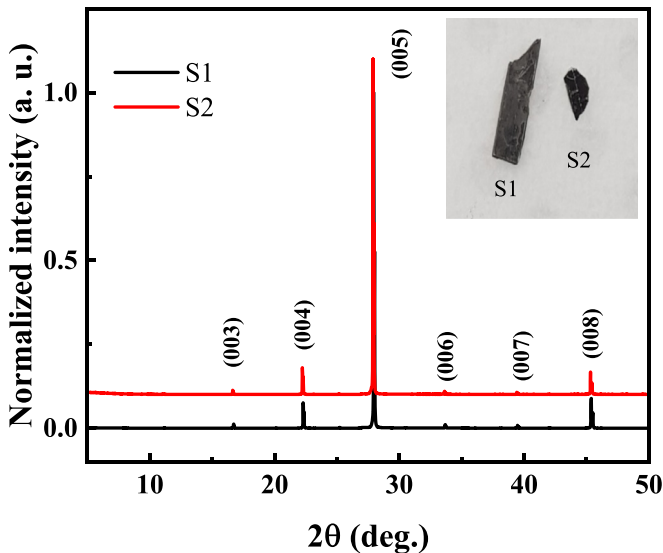
*Email address: jsrhyee@khu.ac.kr

FIG. 1. X-ray diffraction patterns of EuBiTe$_3$ single crystals. The inset shows typical crystals S1 (black line) and S2 (red line).

TABLE II. Atomic coordinates ($\times 10^4$ Å) and equivalent isotropic displacement parameters ($^2 \times 10^3$ Å) of EuBiTe$_3$. U(eq) is defined as one third of the trace of the orthogonalized U^{ij} tensor.

	x	y	z	U(eq)
Bi(1)	2500	2500	1078(1)	34(1)
Eu(1)	7500	7500	3325(1)	18(1)
Te(1)	−2500	−2500	1077(2)	31(1)
Te(2)	2500	2500	2874(2)	16(1)
Te(3)	7500	2500	5003(2)	26(1)

ampoules with molar ratios of Eu:Bi:Te = 1:3:13. The quartz ampoules were heated at 900 °C for 12 h, held for 6 h, and cooled down to 800 °C for 3 h, with subsequent slow cooling to 470 °C for 200 h. The quartz ampoules were decanted, and the samples were separated from the flux using a high-speed centrifuge. The typical size of the obtained samples is $2 \times 2 \times 0.19$ mm^3.

X-ray diffraction (XRD) measurements were performed using Mo $K\alpha$ radiation (0.71073 Å) with a triple-axis four-circle single-crystal diffractometer (D8 Advance, Bruker). The electrical resistivity ρ was measured using the four-point contact method. The magnetization M and specific heat C_p were measured with a physical property measurement system (PPMS-Dynacool 14 T, Quantum Design).

magnetoresistance versus magnetization is explained by the Majumdar-Littlewood (ML) model under a magnetic polaron [19]. Furthermore, we observe that weak antilocalization (WAL) was strongly enhanced for the condition that the electrical current flows parallel to applying magnetic fields ($I \parallel H$), which is contrary to those of typical materials because WAL is enhanced when the direction of the electrical current is perpendicular to the magnetic field direction ($I \perp H$) [21–23]. It can be understood that magnetic polarons along the c axis break time-reversal symmetry (TRS), giving rise to WAL under $I \parallel H$ in the dirty-metal regime [24]. From the angle-resolved magnetoconductivity measurement, we observe a systematic change of WAL with respect to angle between the electrical current and magnetic field directions, showing that EuBiTe$_3$ has potential for applications in magnetic field directional sensors.

II. EXPERIMENTAL DETAILS

Single crystals of EuBiTe$_3$ were synthesized using the Te-flux method. High-purity elements of Eu (99.9%), Bi (99.999%), and Te (99.999%) were loaded in evacuated quartz

III. RESULTS AND DISCUSSION

XRD patterns of single-crystalline EuBiTe$_3$ are revealed in Fig. 1. The inset shows the typical samples what we measured with XRD. It shows well-aligned patterns along the (00l) direction. The crystal refinement data from the triple-axis four-circle single-crystal diffractometer for EuBiTe$_3$ are presented in Table I, where we use the full-matrix least-squares F^2 method. From the refinement, we characterize atomic coordinates and list them in Table II. The crystal structure is orthorhombic with space group *Pmmn*. The crystal structure is presented in Fig. S1 of the Supplemental Material [25]. Bi-Eu-Te slabs are interspaced between Te monolayers. The lattice parameters are $a = 4.517(9)$ Å, $b = 4.614(1)$ Å, and $c = 16.06(3)$ Å, where the lattice volume (334.86 Å^3) is little bit bigger than in the previous report (332.70 Å^3) [13].

TABLE I. Crystal structure refinement of EuBiTe$_3$.

| Parameter	Value	Parameter	Value
Crystal structure	Orthorhombic	Space group	*Pmmn*
a (Å)	4.5179(8)	α	90°
b (Å)	4.6141(8)	β	90°
c (Å)	16.063(3)	γ	90°
V (Å^3)	334.86(10)	Z	2
Density (g/cm^3)	7.376	$F(000)$	604
Absorption coefficient (mm^{-1})	48.187	θ range (deg)	2.536 to 25.495
R indices R_1	0.0546	wR_2 indices	0.1437
Goodness of fit on F^2	1.120	Extinction coefficient	0.0019(6)
Index ranges	$-5 \leqslant h, k \leqslant 5, -19 \leqslant l \leqslant 19$	Completeness to $\theta = 25.242°$	87.2%
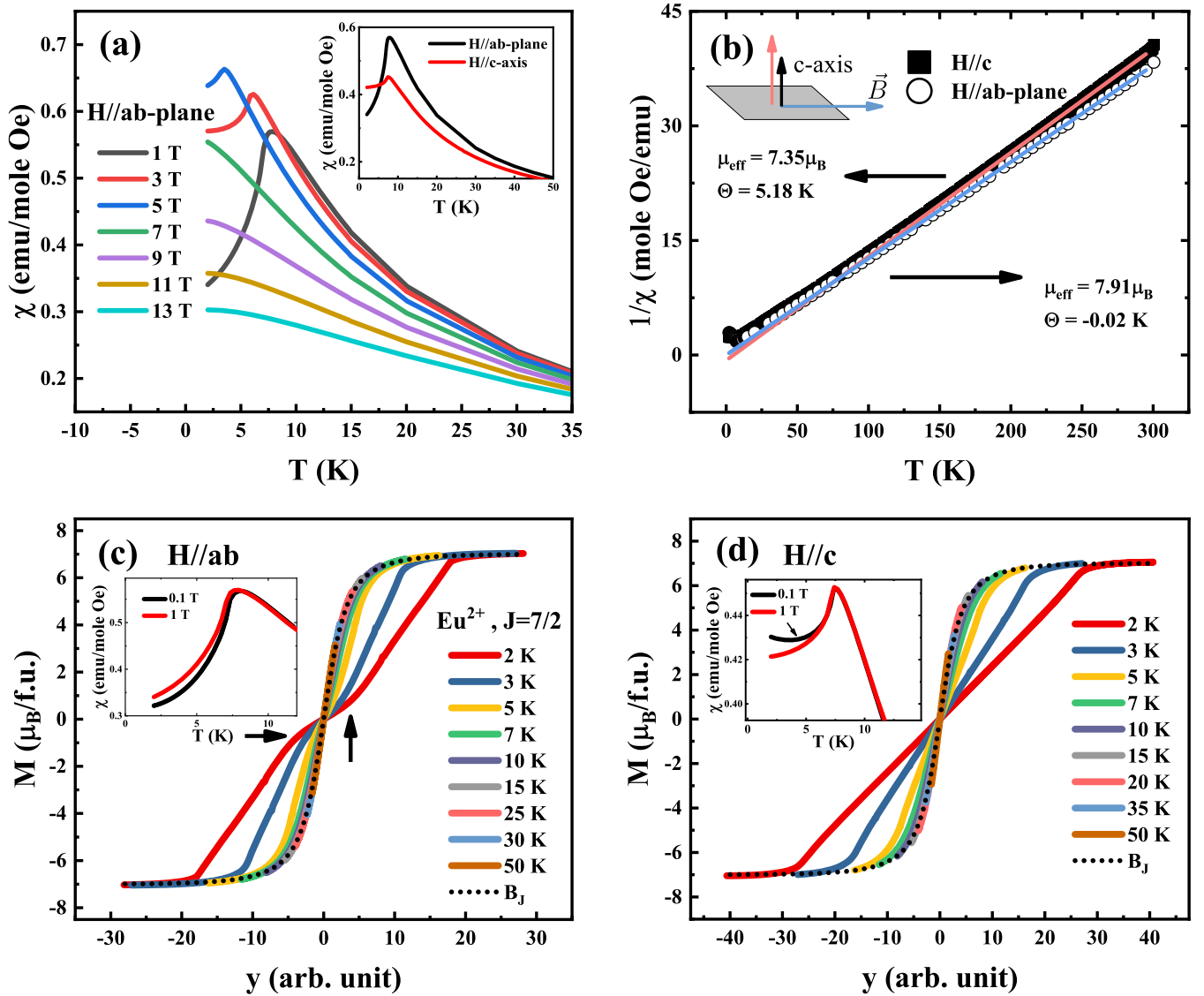
FIG. 2. Magnetic properties of the EuBiTe$_3$ crystal. (a) Temperature-dependent magnetic susceptibility $\chi(T)$ under various magnetic fields as indicated up to $H \leqslant 13$ T. (b) Temperature-dependent inverse magnetic susceptibility under $H = 1$ T for magnetic field along the c axis (black square, pink line) and the ab plane (open circle, sky blue line). Isothermal magnetization versus scaled magnetic field y (defined in the text) for various temperatures, as indicated along the applied magnetic field directions of (c) the ab plane and (d) the c axis. Dotted lines in (c) and (d) are the theoretical fitting by the Brillouin function. Insets of (c) and (d) represent the low-temperature magnetic susceptibility $\chi(T)$ for $H = 0.1$ and 1 T at the respective crystal orientations.

Figure 2(a) shows a temperature-dependent magnetic susceptibility $\chi(T)$ of EuBiTe$_3$ along the $H \parallel ab$ plane. It clearly shows the antiferromagnetic transition at $T_N = 7.6$ K under a magnetic field of $H = 1$ T along the ab plane. The Néel temperatures decrease with increasing magnetic field strength by 6 and 3.5 K for $H = 3$ and 5 T, respectively. The antiferromagnetic order is not observed until 2 K for magnetic field higher than $H = 7$ T. The inset shows the anisotropic magnetic susceptibility $\chi(T)$ under magnetic field along the ab-plane (black line) and axis (red line) for $H = 1$ T. It indicates that the easy axis of spin alignment is on the ab plane because a significant decrease of $\chi(T)$ is observed along the ab plane, while the one of $\chi(T)$ for the c axis shows saturating behavior at low temperature.

The inverse magnetic susceptibility $1/\chi$ in the high-temperature region ($T \geqslant 150$ K) follows well the Curie-Weiss law $1/\chi = (T - \Theta)/C$ for both magnetic field directions of $H \parallel ab$ (open circles) and $H \parallel c$ (black solid rectangles), as presented in Fig. 2(b), where C and Θ are the Curie constant and Weiss temperature, respectively. From the Curie-Weiss fitting, the estimated effective magnetic moments μ_{eff} and Weiss temperatures Θ are $\mu_{eff}^{ab} = 7.9 \, \mu_B$ and $\Theta_{ab} = -0.02$ K for $H \parallel ab$ plane and $\mu_{eff}^c = 7.3 \, \mu_B$ and $\Theta_c = 5.18$ K for $H \parallel c$ axis, respectively. The effective moments are close to that of the Eu^{2+} magnetic moment ($7.9 \, \mu_B$). The Curie-Weiss behavior deviates at low temperature $T \leqslant 150$ K while applying magnetic field along the c axis. The deviation from Curie-Weiss behavior can be caused

by short-range spin correlation [26] and the crystal field effect [27].

Here we can define the frustration parameter f by the ratio between the Weiss temperature Θ and Néel temperature T_N, defined as $f = |\Theta|/T_N$, which denotes the strength of the spin frustration effect [28]. The frustration parameters for two different field directions are $f_c = 0.682$ and $f_{ab} = 0.002$, respectively. The small value of f indicates the relatively strong frustration effect along the ab plane. The positive Θ_c indicates the weak ferromagnetic contribution along the c-axis direction in EuBiTe$_3$.

The magnetization versus magnetic field $M(H)$ at various isothermal temperatures is measured for different crystallographic orientations. In order to see clearly, we scaled the magnetic field by $y = g_J\mu_B J H/k_B T$, which is a scaling factor in the Brillouin function [29]:

$$B_J = \frac{2J+1}{2J}\coth\left(\frac{2J+1}{2J}\right) - \frac{1}{2J}\coth\left(\frac{y}{2J}\right), \quad (1)$$

where $J = 7/2$ for the Eu^{2+} atom. The $M(H)$ data with respect to applied magnetic field are presented in Fig. S2 of the Supplemental Material [25]. For the paramagnetic region, the magnetization versus scaled magnetic field for $H \parallel ab$ [Fig. 2(c)] and $H \parallel c$ axis [Fig. 2(d)] follows very well the Brillouin functional behavior (dotted lines), indicating that the stable Eu^{2+} incorporated the spin alignment. The saturation magnetic moments reach $7\mu_B$ per formula unit, which also supports the stable Eu^{2+} ion. The saturation of magnetization without a metamagnetic transition is also a very interesting property in antiferromagnetic materials. It indicates that the antiferromagnetic spin alignment becomes a ferrimagnetic state not a spin-flip transition when increasing magnetic field up to 6.8 T. For magnetic field higher than 7 T, the ferrimagnetic spin alignment becomes ferromagnetic, which follows the Brillouin functional form of magnetization. The ferrimagnetic state is consistent with the small frustration parameter and ferromagnetic contribution of the Weiss temperature Θ_c from the Curie-Weiss fitting.

The linear relationship with increasing magnetic field up to 7 T at temperatures below T_N is a typical behavior from the antiferromagnetic molecular field interaction. It is noteworthy that the small kink is observed at around $-5 \leqslant y \leqslant 5$ $(-1.5 \leqslant H \leqslant 1.5$ T) at 2 K only along the $H \parallel ab$ direction, which is marked by arrows in Fig. 2(c), while just the linear behavior with magnetic field is shown for the $H \parallel c$ direction [Fig. 2(d)]. This slope change of linear magnetization versus magnetic fields can be characterized by an in-plane spin state transition. This kind of small kink was already reported ori Zn$_{1-x}$Mn$_x$Te compounds [30]. The slope change with magnetic fields can be interpreted as small clusters of ferromagnetic ions, called a magnetic polaron.

The magnetic polaron can be defined by metastable quasiparticles when magnetic ions favor a localized ferromagnetic coupling in the antiferromagnetic or paramagnetic background [15,17]. The coupling is mediated by exchange interaction between the bound carriers which are formed by the impurity state in magnetic semiconductors. In EuBiTe$_3$, the bound carriers may originate from a small amount of Eu^{3+} valence. The small amount of Eu^{3+} valence can be found in

the x-ray photoelectron spectroscopy (XPS) data (not shown here), while any kind of defect or structure dislocation is not detected by the single-crystal XRD refinement.

The magnetic polaron is also observed in the temperature-dependent magnetic susceptibility $\chi(T)$ for different applying magnetic fields, as presented in the insets of Fig. 2. The insets of Figs. 2(c) and 2(d) show $\chi(T)$ curves under magnetic fields of $H = 0.1$ T (black line) and 1 T (red line) along $H \parallel ab$ plane and $H \parallel c$ axis, respectively. From the inset of Fig. 2(d), we can easily recognize a small upturn for $H \parallel c$ axis under $H = 0.1$ T, indicating a complex spin structure including spin canting. In many cases, the small upturn of $\chi(T)$ is observed in samples that contain ferromagnetic impurities. We do not find any impurity phases from the x-ray diffraction and single-crystalline x-ray refinement with the four-circle diffractometer. On the other hand, the magnetization versus magnetic field shows stable antiferromagnetic behavior that linearly increases with applying magnetic field. The small upturn of $\chi(T)$ with the stable antiferromagnetic background along the c axis may be related to the magnetic polaron. The magnetic polaron is a state of bound ferromagnetic clusters under an antiferromagnetic background. The small upturn of $\chi(T)$ is not observed along the ab-plane direction, as plotted in the inset of Fig. 2(c). The magnetic polaron contribution along the $H \parallel c$ direction is consistent with the ferromagnetic Weiss temperature Θ_c along the c axis.

The small upturn of magnetic susceptibility at low temperature under the antiferromagnetic background can give rise to the formation of a bound magnetic polaron. In order to elucidate the magnetic property contributions to the thermal property, we measured the temperature-dependent heat capacity $C_p(T)$ as presented in Fig. 3(a). There is a sharp λ-type transition at $T_N = 7.6$ K, confirming the long-range antiferromagnetic transition. $C_p(T)$ can be fitted with the Debye model $C_p = \gamma T + \beta T^3$, where γ is the Sommerfeld coefficient and β is the lattice contribution to heat capacity, where $\gamma = 503.38$ mJ mol^{-1} K^{-2} and $\beta = 1.96$ mJ mol^{-1} K^{-4}. The Sommerfeld coefficient is exceedingly large compared with the antiferromagnetic insulator Cd$_2$Os$_2$O$_7$ ($\gamma = 1.08$ mJ mol^{-1} K^{-2}) [31], the metallic charge density wave system SmNiC$_2$ ($\gamma = 8.0$ mJ mol^{-1} K^{-2}) [32], and even the heavy-fermion compound CePtAl$_4$Ge$_2$ ($\gamma = 201.38$ mJ mol^{-1} K^{-2}) [33]. The large value of γ can be caused by strong disorder [34], strong correlation between electron and orbital ordering [35], and strong ferromagnetic fluctuation [36]. It is noteworthy that EuBiTe$_3$ shows insulating behavior in the electrical transport, as presented in Fig. 4(a). Therefore, the large Sommerfeld coefficient is not caused by the enhancement of effective mass but comes from the strong ferromagnetic fluctuation. The high Sommerfeld coefficient from strong ferromagnetic fluctuation in an electrical insulator is also observed in Cu$_2$(VO$_4$)(OH), showing a canted antiferromagnetic ordering with weak spin frustration arising from the competition between antiferromagnetic and ferromagnetic interactions [37].

In order to extract the magnetic contribution of heat capacity C_{mag}, we subtracted the lattice contribution of C_p, as depicted in the inset of Fig. 3(a) (red line). The magnetic contribution of heat capacity versus temperature $C_{mag}(T)$ in the vicinity of antiferromagnetic transition is depicted in
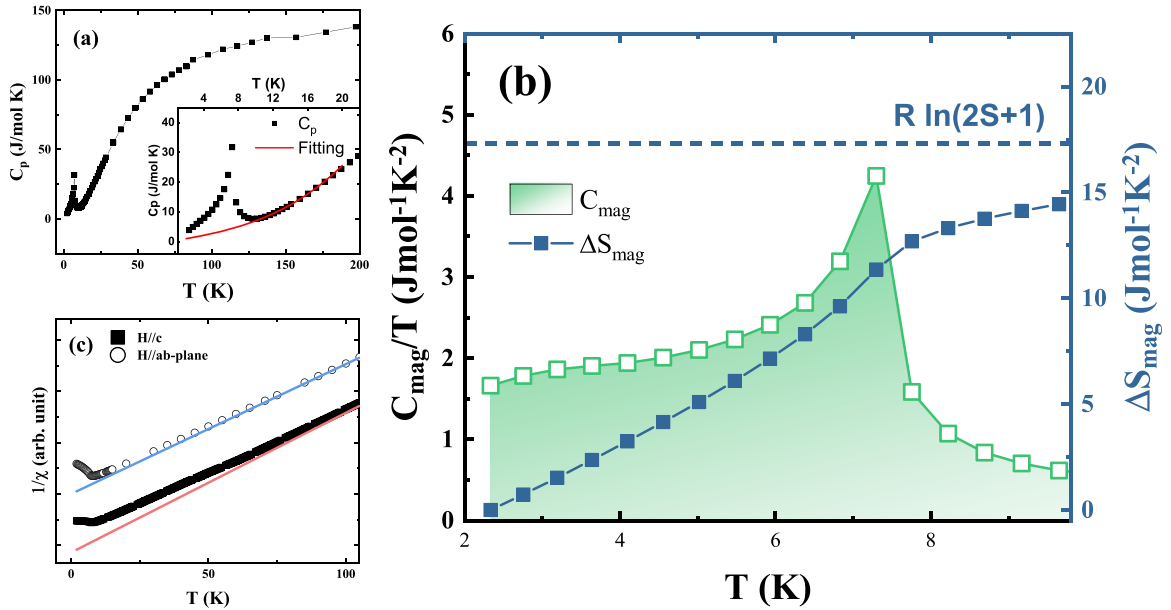
FIG. 3. (a) Temperature-dependent specific heat C_p of EuBiTe$_3$. The inset shows an expanded plot of C_p at low temperatures ($T \leqslant 25$ K). The red line is the fitting result from $C_p(T) = \gamma T + \beta T^3$. (b) Temperature-dependent magnetic heat capacity divided by temperature C_{mag}/T, where C_{mag} is subtracted from the electronic and lattice heat capacity [inset of (a); shaded region, left axis] and magnetic entropy change ΔS_{mag} (right axis). The dashed line is the value of $R\ln(2S+1)$ for $S = 7/2$. (c) Temperature-dependent inverse magnetic susceptibility $\chi^{-1}(T)$ for different crystalline orientations of $H \parallel c$ axis (black square, sky blue line) and $H \parallel ab$ plane (open circle, pink line).

Fig. 3(b). From the magnetic specific heat, we can obtain the magnetic entropy from the relation $\Delta S_{mag} = \int (C_{mag}/T)dT$. The estimated value of magnetic entropy is 14.44 J mol^{-1} K^{-2}, which is about 83% of theoretical value given by Boltzmann's law, $\Delta S = R\ln(2S+1) \approx 17.29$ J mol^{-1} K^{-2} for an $S = 7/2$ system, as presented in Fig. 3(b) (right axis). The estimated value of S_{mag} lower than theoretical expectation implies that the magnetic transition is not purely from the long-range magnetic interaction but from the competition between long-range and short-range interactions.

The competing behavior between long-range and short-range magnetic interactions can be identified in the temperature-dependent inverse magnetic susceptibility $1/\chi(T)$, as depicted in Fig. 3(c). For $H \parallel ab$ plane (open circles), $1/\chi(T)$ shows linear behavior with temperature down to the antiferromagnetic transition temperature, indicating a typical Curie-Weiss law. On the other hand, for the inverse magnetic susceptibility along $H \parallel c$ axis (solid squares), the linear relationship deviates at high temperature (about 100 K), which is a typical signature of short-range correlation [38]. The anisotropic behavior on the temperature-dependent inverse magnetic susceptibility suggests that a short-range correlation is more significant along $H \parallel c$ axis than the case of $H \parallel ab$ plane. One possibility of short-range correlation with ferromagnetic fluctuation under the antiferromagnetic background is the existence of a bound magnetic polaron.

When we measure the temperature-dependent electrical resistivity $\rho(T)$, it exhibits unconventional behavior with temperature. The inset of Fig. 4 presents a semilog plot of electrical resistivity (log scale) versus temperature (linear scale). Evidently, it is an insulator at low temperature with an order of 10 kΩ cm at 2 K, but it does not follow conventional

temperature dependence of a semiconductor: $\rho = \rho_0 e^{-aT}$. For applied magnetic fields, $\rho(T)$ is decreased with increasing magnetic fields at low temperatures, indicating a negative magnetoresistance (MR). The negative magnetoresistance at high magnetic fields ($H \geqslant 3$ T) can be understood by the decrease of electron-spin scattering due to the evolution of spin alignment with increasing magnetic field from the antiferromagnetic state, as shown in Fig. 2(a).

The isothermal magnetoresistance $[\rho(H) - \rho(0)]/\rho(0)$ with respect to applying magnetic field up to 13 T along the c-axis direction is shown in Fig. 4(b) at temperatures below 50 K, as indicated. At low magnetic fields ($H \leqslant 600$ Oe), the MR is increased with increasing magnetic fields for $T \leqslant 7$ K, which might be associated with antiferromagnetic transition. For magnetic fields higher than 600 Oe, the MR significantly decreased with increasing magnetic fields at low temperatures. Especially, a significant drop in MR saturates at $H \geqslant 8$ T for $T = 2$ and 3 K. The negative MR at high magnetic fields is increased with increasing temperatures but still remains a negative value for $T \leqslant 50$ K.

The sharp increase of MR at low magnetic field and significant decrease of MR at higher magnetic field ($H \geqslant 600$ Oe) at low temperature ($T \leqslant 7$ K) are similar to the crossover between WL and WAL [39,40]. Recent investigation shows that WAL is observed in Dirac semimetals and topological insulators, induced by a relative Berry phase with respect to time-reversed paths [41,42]. The weak localization is generally observed in trivial magnetic materials with broken time-reversal symmetry. In the magnetic ion-doped Bi$_2$Se$_3$, a weak antilocalization to weak localization crossover was observed with respect to doping, temperature, and magnetic fields [39]. However, the topologically driven WAL to WL crossover is not likely in this compound because this compound already
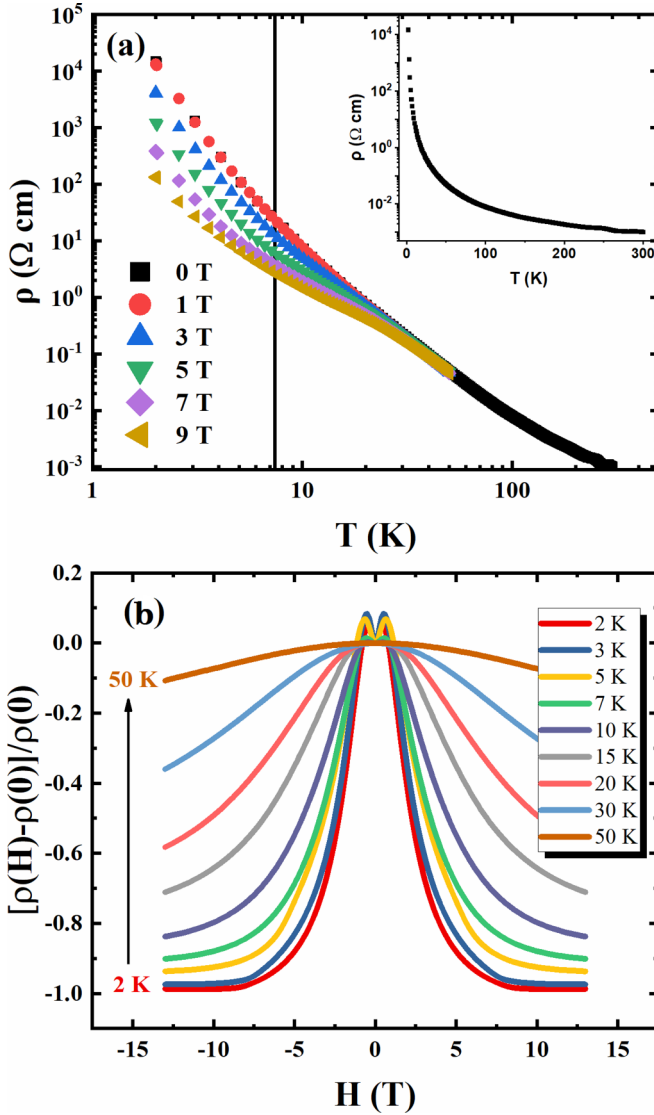
FIG. 4. (a) Log-log plot of electrical resistivity versus temperature $\rho(T)$ under various magnetic fields as indicated. The vertical line is the Néel temperature. The inset shows the semilog plot of electrical resistivity versus temperature without magnetic field. (b) Isothermal magnetoresistance $[\rho(H) - \rho(0)]/\rho(0)$ versus magnetic field ranging from $-13\,\mathrm{T} \leqslant H \leqslant 13\,\mathrm{T}$ at the temperature, as indicated below 50 K.

has broken time-reversal symmetry; in other words, it is a topologically trivial magnetic material.

This WAL to WL crossover behavior can be understood by the competition between long-range antiferromagnetic order and the short-range ferromagnetic cluster, namely, a bound magnetic polaron. At low temperature and low magnetic fields, the antiferromagnetic ordering gives rise to positive magnetoresistance, while ferromagnetic clusters evolve when we apply magnetic fields. Thermal activation at temperatures higher than the Néel temperature can also maintain short-range magnetic interaction, giving rise to a bound magnetic polaron. The negative magnetoresistance at temperatures higher than T_N (up to 50 K) is consistent with the assumption of short-range ferromagnetic cluster.
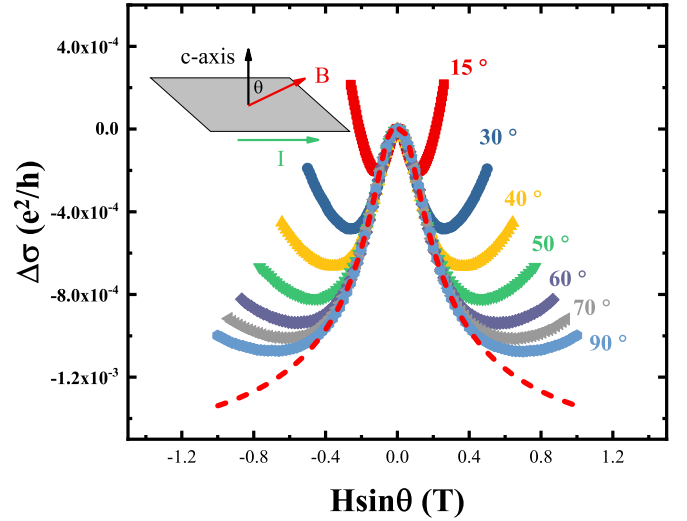

FIG. 5. Angle-resolved magnetoresistance $\Delta\sigma$ with respect to scaled magnetic field $H \sin\theta$ for respective angles θ between the magnetic field direction and the c axis. The dashed line represents the longitudinal weak antilocalization fitting with the Al'tshuler and Aronov model.

In order to elucidate the exotic MR behavior at low temperature and low magnetic field, we measured angle-resolved magnetoresistance at $T = 2$ K, as depicted in Fig. 5. In the case of WAL in topological insulators, the two-dimensional surface Dirac fermions gives rise to a WAL signal with a dip at low magnetic field. The WAL signal is diminished by applying magnetic field along the in-plane direction [21,23]. On the other hand, in this compound, the (WAL-like) crossover behavior becomes significant for applying magnetic field to the in-plane direction. It strongly indicates that the abnormal magnetoresistance is caused by the magnetic polaron, as discussed below.

As we mentioned above, magnetic polarons in EuBiTe$_3$ prefer ferromagnetic interaction along the c-axis direction (AF or canted AF interaction along the ab plane). The WAL can exist only under the TRS; however, the ferromagnetic alignment breaks the TRS and gives additional magnetic flux. The additional magnetic flux destroys the coherence of the phase in the electronic wave function when electrons move through a closed path on the ab plane; thereby, the WAL diminishes when applying magnetic field along the c axis. On the other hand, because of the absence of additional internal net magnetic flux due to antiferromagnetic interaction along the ab plane, the closed electron path out of the plane can have a phase coherence length longer than the in-plane one.

The WAL for applying magnetic field along the out-of-plane direction in a two-dimensional surface state is explained by the Hikami-Larkin-Nagaoka (HLN) theory as following equation [43]:

$$\Delta\sigma(B) = \alpha \frac{e^2}{2\pi^2 \hbar} \left[\psi \left(\frac{1}{2} + \frac{\hbar}{4eBL_\phi^2} \right) - \ln \left(\frac{\hbar}{4eBL_\phi^2} \right) \right], \quad (2)$$

where $\psi(x)$ is the digamma function, L_ϕ is the phase coherence length, and α is the parameter that is given by $-1/2$ per surface channel. On the other hand, when we apply

magnetic field along the in-plane direction, the MR behavior becomes complicated, so several models were proposed in terms of sample thickness [24]. In the dirty-metal regime, where the mean-free path l_e is much smaller than sample thickness d, the MR behavior is described by the Al'tshuler and Aronov (AA) model [44]. In the case of the pure-metal regime ($l_e \gg d$), in contrast, the MR can be explained by the Dugaev-Khmelnitskii (DK) model [45]. The crossover between AA and DK was described by Beenakker and van Houten [46]. Because the HLN model describes only a WAL under magnetic field along the out-of-plane direction, the generalized longitudinal magnetoresistance with quantum correction term from the above models can be written as [24]

$$\Delta\sigma_{\parallel}(B) \simeq -\alpha \frac{e^2}{2\pi^2\hbar} \ln\left(1 + \frac{\beta e d^2}{4\hbar B_\phi} B^2\right), \qquad (3)$$

where $\Delta\sigma_{\parallel}(B) \equiv \sigma_{xx}(B_{\parallel}) - \sigma_{xx}(0)$, α is $1/2$ for WAL and -1 for WL at each surface channel, B_ϕ is the dephasing field, and d is the thickness of samples.

From the above general equation, each model is characterized by the parameter β. The parameter β is $1/3$ for the AA regime ($l_e \ll d$) and $1/16$ ($d \ll l_e$) for the DK regime. When we take into account that our sample is not a film but a bulk slab with a thickness of 0.19 mm, the insulating nature of electrical transport suggests that the mean-free path is much smaller than the sample thickness. Therefore, we surmise that the MR of EuBiTe$_3$ is in the AA regime. The red dashed line in Fig. 5 is the calculation result of the longitudinal MR curve ($H \parallel$ in plane) from the WAL in the AA regime, which agrees fairly well with experiment.

In dilute magnetic semiconductors with a typical magnetic polaron, the negative magnetoresistance is observed over a wide temperature range at temperatures higher than T_N. In that case, the magnetoresistance is linearly scaled by $(m/m_{sat})^2$ within the ML model, where m is the magnetization and m_{sat} is the saturation magnetization at high magnetic field [19]. This model is adapted with a self-trapped magnetic polaron system regardless of the specific magnetic interaction [47]. Furthermore, because the local distribution of magnetic polarons can be treated as random hopping sites, we can expect electrical transport in terms of random hopping in a semiconducting background. The random scattering of transport carriers allows a positive correction term in the resistivity formalism. When we apply the magnetic field, the carrier acquires an additional phase at each scattering processes, and the resistivity is decreased when applying magnetic fields, which is called weak localization [41,48].

The increasing MR for low magnetic fields and low temperatures corresponds to the WAL. At high magnetic fields and high temperatures, the bound magnetic polaron can increase in size, giving rise to the decrease of hopping energy, thus resulting in the negative magnetoresistance. This magnetic polaron scenario within the ML model fits relatively well, as presented in Fig. 5(a). The negative magnetoresistance linearly fits well with the ML model at the paramagnetic state (in the range of $20\,\text{K} \leqslant T \leqslant 50\,\text{K}$). Within the argument of the ML model, the slope is a function of correlation length ξ_0, with $\Delta\rho/\rho \approx (1/2k_F\xi_0)^2 (m/m_{sat})^2$, where ξ_0 is the
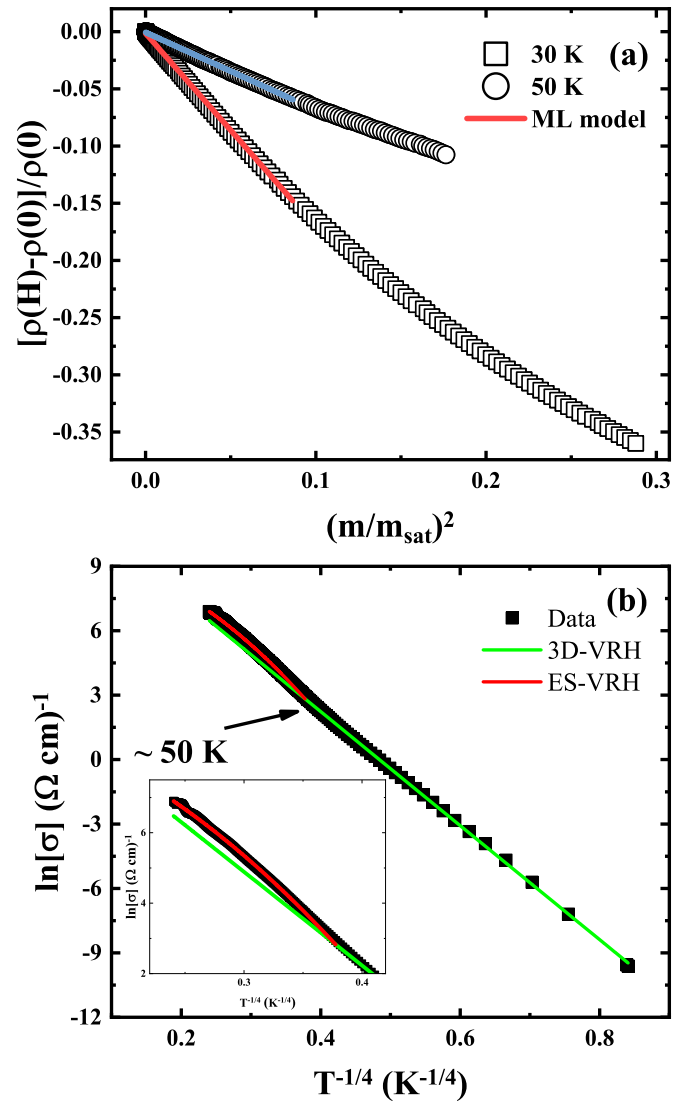

FIG. 6. (a) Magnetoresistance versus $(m/m_{sat})^2$ at two different temperatures of 30 K (open squares) and 50 K (open circles). Lines are fitted results with the Majumdar and Littlewood (ML) model. (b) Logarithmic electrical conductivity versus $T^{-1/4}$ of the EuBiTe$_3$ crystal without magnetic field. Bright green and red lines represent three-dimensional variable range hopping (VRH) and Efros-Shklovskii-type (ES) transport, respectively.

order of separation between ferromagnetic clusters. In our system, the correlation length between ferromagnetic clusters increases with decreasing temperature.

The localized state of the bound magnetic polaron also affects the electrical transport even under zero magnetic field. The random distribution of polaronic hopping sites may give rise to three-dimensional Mott variable range hopping (VRH) as the relation $\sigma = \sigma_0 \exp(-T_0/T)^n$ at sufficiently low temperature, where $n = 1/(d+1)$ for d-dimensional hopping and T_0 is the Mott temperature correlated with the localization length, density of states, and electronic structure [49]. Efros and Shklovskii (ES) argue that when long-range Coulomb interaction is strong between localized electrons, the electrical conductivity follows $n = 1/2$ in the ES VRH regime [50,51].

Figure 6(b) presents the logarithmic electrical conductivity versus $T^{-1/4}$. At low temperature $T \leqslant 50$ K, it follows the three-dimensional Mott VRH very well (sky blue line). On the other hand, the logarithmic electrical conductivity follows the ES-type VRH model such that $n = 1/2$ in the high-temperature range ($T \geqslant 52$ K). It is not likely to be the one-dimensional VRH because it has three-dimensional bulk crystals. Therefore, we believe that transport is dominated by two distinguished physical origins in different temperature regions. The ES VRH model indicates long-range Coulomb interaction at high temperature ($T \geqslant 50$ K), and it evolves to random hopping of electronic transport via the three-dimensional VRH mechanism at low temperature ($T \leqslant 50$ K). The temperature range is also consistent with the short-range magnetic fluctuation in the inverse magnetic susceptibility with temperature, as shown in the inset of Fig. 3(b). Therefore, the existence of the magnetic polaron is attributed to the abnormal behaviors of $\chi(T)$, $M(H)$, negative MR, and the electrical transport properties along the c direction.

In the ES VRH mechanism, however, long-range Coulomb interaction should open a band gap near the Fermi level. It is very interesting that EuBiTe$_3$ should have one hole per formula unit. Typically, many compounds containing Bi and Te, such as Bi$_2$Te$_3$ and BiTeI, have charge valences with Bi^{3+} and Te^{2-}, respectively. So we expected that one valence electron would leave (EuBiTe$_3$)$^{-1}$ because Eu has a Eu^{2+} state, as we confirmed by XPS measurement. Although the metallic behavior is expected when we take into account the charge valance, $\sigma(T)$ of EuBiTe$_3$ shows insulating behavior with VRH transport. One possible scenario for the insulating behavior of EuBiTe$_3$ is the Mott-type insulator due to strong Coulomb interaction. It is reasonable because $\sigma(T)$ is described by the ES VRH transport at high temperatures. It is well known that many half-filling systems ($S = 1/2$) open a band gap due to strong Coulomb interaction, which is the Mott insulator [49,52,53]. The strong Coulomb interaction and VRH transport in electrical transport suggest the possibility that EuBiTe$_3$ ($S = 7/2$) is a Mott insulator, which should be investigated in further research.

IV. CONCLUSIONS

In summary, we synthesized a EuBiTe$_3$ single crystal and investigated the magnetic, thermal, and electrical transport properties. The $M(T)$ and $M(H)$ curves showed antiferromagnetic interaction along the ab plane with a stable Eu^{2+} ion. Short-range ferromagnetic interaction, in other words, a bound magnetic polaron, was revealed along the c axis by the small upturn of $\chi(T)$ at low temperature, the deviation from the Curie-Weiss law, and a magnetic entropy smaller than the one for stable Eu^{2+}.

The magnetic polaron was also supported by the unconventional negative magnetoresistance. The negative MR is suppressed with increasing temperature due to a decrease of the magnetic polaron size at high temperature. Interestingly, we observed a WAL at low temperature in the low-magnetic-field region. From the angle-resolved MR measurement, the WAL becomes significant for applying magnetic field to the in-plane direction. We can understand that the magnetic polaron along the c axis introduces an additional magnetic phase which breaks time-reversal symmetry. The WAL of longitudinal magnetoconductivity is well described by the Al'tshuler and Aronov model, which is reasonable in bulk crystals (small coherence length compared with sample size). The magnetoresistance is scaled by $(m/m_{sat})^2$ within the Majumdar and Littlewood model. It also supports the magnetic polaron formation over a wide temperature range below 50 K.

Even though EuBiTe$_3$ should have one hole per formula unit, the electrical conductivity exhibited strong localized insulating behavior. At high temperature ($T \geqslant 52K$), the electrical conductivity follows the Efros-Shklovskii-type variable range hopping model, while $\sigma(T)$ follows the three-dimensional VRH model at low temperatures ($T \leqslant 50K$). The change in transport mechanism can be attributed to the formation of a magnetic polaron in a similar temperature range. The ES-type VRH model indicates that EuBiTe$_3$ has strong Coulomb interaction. Therefore, the insulating behavior of electrical transport in the compound can originate from a Mott-type insulator.

[1] H. Zhang, C.-X. Liu, X.-L. Qi, X. Dai, Z. Fang, and S.-C. Zhang, Nat. Phys. **5**, 438 (2009).

[2] Y. L. Chen, J. G. Analytis, J.-H. Chu, Z. K. Liu, S.-K. Mo, X. L. Qi, H. J. Zhang, D. H. Lu, X. Dai, Z. Fang, S.-C. Zhang, I. R. Fisher, Z. Hussain, and Z.-X. Shen, Science **325**, 178 (2009).

[3] Y. Xia, D. Qian, D. Hsieh, L. Wray, A. Pal, H. Lin, A. Bansil, D. Grauer, Y. S. Hor, R. J. Cava, and M. Z. Hasan, Nat. Phys. **5**, 398 (2009).

[4] J. E. Moore, Nature (London) **464**, 194 (2010).

[5] M. Dzero, K. Sun, V. Galitski, and P. Coleman, Phys. Rev. Lett. **104**, 106408 (2010).

[6] D. J. Kim, J. Xia, and Z. Fisk, Nat. Mater. **13**, 466 (2014).

[7] R. S. K. Mong, A. M. Essin, and J. E. Moore, Phys. Rev. B **81**, 245209 (2010).

[8] R. A. Müller, N. R. Lee-Hone, L. Lapointe, D. H. Ryan, T. Pereg-Barnea, A. D. Bianchi, Y. Mozharivskyj, and R. Flacau, Phys. Rev. B **90**, 041109(R) (2014).

[9] S. Raghu, X. L. Qi, C. Honerkamp, and S.-C. Zhang, Phys. Rev. Lett. **100**, 156401 (2008).

[10] H.-M. Guo, G. Rosenberg, G. Refael, and M. Franz, Phys. Rev. Lett. **105**, 216601 (2010).

[11] B. Yan, H. J. Zhang, C. X. Liu, X. L. Qi, T. Frauenheim, and S. C. Zhang, Phys. Rev. B **82**, 161108(R) (2010).

[12] J. Liu and D. Vanderbilt, Phys. Rev. B **90**, 155316 (2014).

[13] Y. Y. Niu, D. Wu, L. Shen, and B. Wang, Phys. Status Solidi RRL **9**, 735 (2015).

[14] Y. Niu, B. Wang, J. Chen, and D. Wu, J. Mater. Chem. C **6**, 713 (2018).

[15] V. G. Storchak, O. E. Parfenov, J. H. Brewer, P. L. Russo, S. L. Stubbs, R. L. Lichti, D. G. Eshchenko, E. Morenzoni, T. G. Aminov, V. P. Zlomanov, A.A. Vinokurov, R. L. Kallaher, and S. von Molnár, Phys. Rev. B **80**, 235203 (2009).

[16] M. Umehara, J. Phys. Soc. Jpn. **50**, 1082 (1981).

[17] A. C. Durst, R. N. Bhatt, and P. A. Wolff, Phys. Rev. B **65**, 235205 (2002).

[18] M. J. Calderón, L. G. L. Wegener, and P. B. Littlewood, Phys. Rev. B **70**, 092408 (2004).

[19] P. Majumdar and P. B. Littlewood, Nature (London) **395**, 479 (1998).

[20] H. D. Zhou, E. S. Choi, J. A. Souza, J. Lu, Y. Xin, L. L. Lumata, B. S. Conner, L. Balicas, J. S. Brooks, J. J. Neumeier, and C. R. Wiebe, Phys. Rev. B **77**, 020411(R) (2008).

[21] J. J. Cha, D. Kong, S.-S. Hong, J. G. Analytis, K. Lai, and Y. Cui, Nano Lett. **12**, 1107 (2012).

[22] W. Ning, F. Kong, Y. Han, H. Du, J. Yang, M. Tian, and Y. Zhang, Sci. Rep. **4**, 7086 (2014).

[23] G. Xu, W. Wang, X. Zhang, Y. Du, E. Liu, S. Wang, G. Wu, Z. Liu, and X. X. Zhang, Sci. Rep. **4**, 5709 (2014).

[24] C. J. Lin, X. Y. He, J. Liao, X. X. Wang, V. Sacksteder, W. M. Yang, T. Guan, Q. M. Zhang, L. Gu, G. Y. Zhang, C. G. Zeng, X. Dai, K. H. Wu, and Y. Q. Li, Phys. Rev. B **88**, 041307(R) (2013).

[25] See Supplemental Material at http://link.aps.org/supplemental/10.1103/PhysRevB.100.024433 for crystal structure of EuBiTe$_3$, temperature dependent magnetization versus magnetic field, and CIF file of EuBiTe$_3$ single crystal X-ray refinement.

[26] E. E. Barton and H. Claus, Phys. Lett. A **30**, 502 (1969).

[27] M.-D. Guo, A. T. Aldred, and S.-K. Chan, J. Phys. Chem. Solids **48**, 229 (1987).

[28] A. P. Ramirez, Annu. Rev. Mater. Sci. **24**, 453 (1994).

[29] S. Blundell, *Magnetism in Condensed Matter* (Oxford University Press, Oxford, 2001).

[30] G. Barilero, C. Rigaux, N. H. Hau, J. C. Picoche, and W. Giriat, Solid State Commun. **62**, 345 (1987).

[31] D. Mandrus, J. R. Thompson, R. Gaal, L. Forro, J. C. Bryan, B. C. Chakoumakos, L. M. Woods, B. C. Sales, R. S. Fishman, and V. Keppens, Phys. Rev. B **63**, 195104 (2001).

[32] J. H. Kim, J.-S. Rhyee, and Y. S. Kwon, Phys. Rev. B **86**, 235101 (2012).

[33] S. Shin, P. F. S. Rosa, F. Ronning, J. D. Thompson, B. L. Scott, S. Lee, H. Jang, S.-G. Jung, E. Yun, H. Lee, E. D. Bauer, and T. Park, J. Alloys Compnd. **738**, 550 (2018).

[34] E. Svanidze, A. Amon, Yu. Prots, A. Leithe-Jasper, and Yu. Grin, Phys. Rev. B **97**, 115148 (2018).

[35] D. Jang, P. Y. Portnichenko, A. S. Cameron, G. Friemel, A. V. Dukhnenko, N. Y. Shitsevalova, V. B. Filipov, A. Schneidewind, A. Ivanov, D. S. Inosov, and M. Brando, npj Quantum Mater. **2**, 62 (2017).

[36] P. Limelette, H. Muguerra, and S. Hébert, Phys. Rev. B **82**, 035123 (2010).

[37] S. Y. Zhang, Z. Z. He, M. Yang, W. B. Guo, and Y. Y. Tang, Dalton Trans. **43**, 3521 (2014).

[38] S. Derakhshan, J. E. Greedan, and L. M. D. Cranswick, Phys. Rev. B **77**, 014408 (2008).

[39] M. Liu, J. Zhang, C.-Z. Chang, Z. Zhang, X. Feng, K. Li, K. He, L.-l. Wang, X. Chen, X. Dai, Z. Fang, Q.-K. Xue, X. Ma, and Y. Wang, Phys. Rev. Lett. **108**, 036805 (2012).

[40] W. H. Shon and J.-S. Rhyee, J. Phys.: Condens. Matter. **27**, 025502 (2015).

[41] H.-Z. Lu and S.-Q. Shen, Phys. Rev. B **84**, 125138 (2011).

[42] H.-T. He, G. Wang, T. Zhang, I.-K. Sou, G. K. L. Wong, J.-N. Wang, H.-Z. Lu, S.-Q. Shen, and F.-C. Zhang, Phys. Rev. Lett. **106**, 166805 (2011).

[43] S. Hikami, A. I. Larkin, and Y. Nagaoka, Prog. Theor. Phys. **63**, 707 (1980).

[44] B. L. Altshuler and A. G. Aronov, JETP Lett. **33**, 499 (1981).

[45] V. K. Dugaev and D. E. Khmelnitskii, Zh. Eksp. Teor. Fiz. **86**, 1784 (1984).

[46] C. W. J. Beenakker and H. van Houten, Phys. Rev. B **38**, 3232 (1988).

[47] P. B. Littlewood, Acta Phys. Pol. A **97**, 7 (2000).

[48] T. Koga, J. Nitta, T. Akazaki, and H. Takayanagi, Phys. Rev. Lett. **89**, 046801 (2002).

[49] N. F. Mott, *Metal-Insulator Transitions* (Taylor and Francis, London, 1990).

[50] A. L. Efros and B. I. Shklovskii, J. Phys. C **8**, L49 (1975).

[51] K. G. Raj and P. A. Joy, Phys. Chem. Chem. Phys. **17**, 16178 (2015).

[52] D. B. McWhan, A. Menth, J. P. Remeika, W. F. Brinkman, and T. M. Rice, Phys. Rev. B **7**, 1920 (1973).

[53] R. Pocha, D. Johrendt, B. Ni, and M. M. Abd-Elmeguid, J. Am. Chem. Soc. **127**, 8732 (2005).